

Verification of the Cardinal Multiphysics Solver for 1-D Coupled Heat Transfer and Neutron Transport

Lewis I. Gross¹, April J. Novak^{2,3}, Patrick Shriwise^{3,1}, and Paul P.H. Wilson¹

University of Wisconsin-Madison¹, University of Illinois Urbana-Champaign², Argonne
National Lab³

August 16, 2022



WISCONSIN
UNIVERSITY OF WISCONSIN-MADISON

Outline

① Introduction

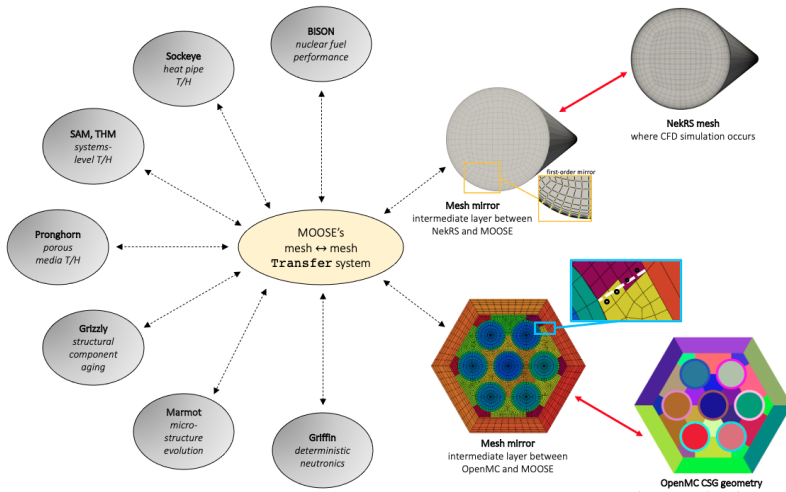
② Analytical Benchmark

③ Computational Model

④ Results and Discussion

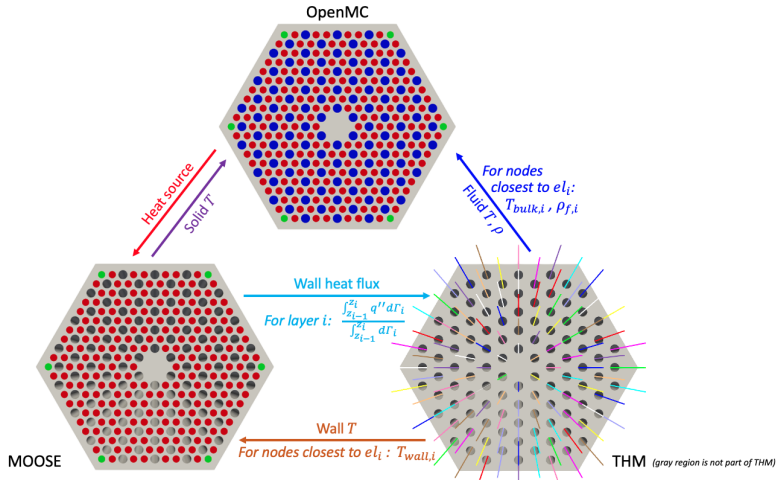


Cardinal [1] wraps OpenMC [2] and NekRS [3] into the MOOSE framework [4].



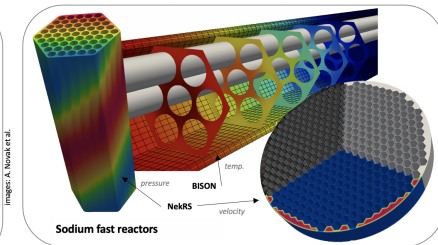
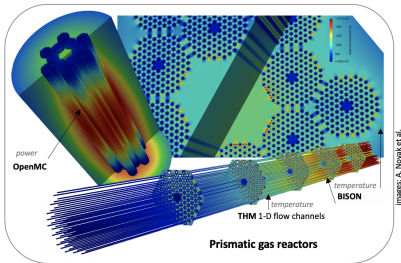


Cardinal: A Modern Multiphysics Software

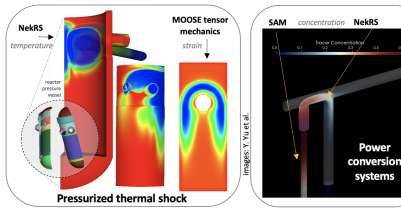




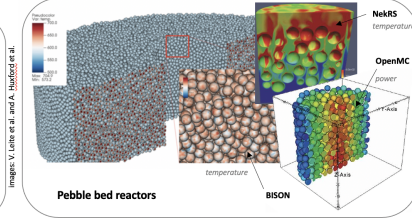
Application of Cardinal to Model Advanced Reactors



Images: A. Novak et al.



Images: V. Lette et al. and A. Huxford et al.



Images: P. Fischer et al. and E. Merabt et al.



Modern Multiphysics Simulation and the Importance of V&V



Modern Multiphysics Simulation and the Importance of V&V

- All software tools require Verification and Validation (V&V) to ensure quality results.



Modern Multiphysics Simulation and the Importance of V&V

- All software tools require Verification and Validation (V&V) to ensure quality results.
 - Verification involves basic numerical checks of a solver, as well as comparison to other codes or to physics theory.



Modern Multiphysics Simulation and the Importance of V&V

- All software tools require Verification and Validation (V&V) to ensure quality results.
 - Verification involves basic numerical checks of a solver, as well as comparison to other codes or to physics theory.
 - Validation is the comparison of simulations to experimental results.



Modern Multiphysics Simulation and the Importance of V&V

- All software tools require Verification and Validation (V&V) to ensure quality results.
 - Verification involves basic numerical checks of a solver, as well as comparison to other codes or to physics theory.
 - Validation is the comparison of simulations to experimental results.
- Verification against analytical benchmarks allow measurement of true error.



Modern Multiphysics Simulation and the Importance of V&V

- All software tools require Verification and Validation (V&V) to ensure quality results.
 - Verification involves basic numerical checks of a solver, as well as comparison to other codes or to physics theory.
 - Validation is the comparison of simulations to experimental results.
- Verification against analytical benchmarks allow measurement of true error.
- Greisheimer and Kooreman presented a 1-D analytical benchmark featuring coupled heat transfer and neutron transport [5].

Analytical Benchmark





Analytical Benchmark

- This analytical benchmark includes



Analytical Benchmark

- This analytical benchmark includes
 - S_2 transport: particles restricted to the $\pm x$ direction.



Analytical Benchmark

- This analytical benchmark includes
 - S_2 transport: particles restricted to the $\pm x$ direction.
 - Doppler-broadening

$$\sigma_t(x) = \sigma_{t,0} \sqrt{\frac{T_0}{T(x)}} \quad (1)$$



Analytical Benchmark

- This analytical benchmark includes
 - S_2 transport: particles restricted to the $\pm x$ direction.
 - Doppler-broadening

$$\sigma_t(x) = \sigma_{t,0} \sqrt{\frac{T_0}{T(x)}} \quad (1)$$

- 1-D thermal expansion

$$\rho(x) = \rho_0 \sqrt{\frac{T_0}{T(x)}} \quad (2)$$



Analytical Benchmark

- This analytical benchmark includes
 - S_2 transport: particles restricted to the $\pm x$ direction.
 - Doppler-broadening

$$\sigma_t(x) = \sigma_{t,0} \sqrt{\frac{T_0}{T(x)}} \quad (1)$$

- 1-D thermal expansion

$$\rho(x) = \rho_0 \sqrt{\frac{T_0}{T(x)}} \quad (2)$$

- Using (1) and (2) gives a Doppler-broadened, macroscopic, total cross section that accounts for changes in density due to temperature as

$$\Sigma_t(x) = \frac{\rho_0 \sigma_{t,0} N_A}{A} \frac{T_0}{T(x)} \equiv \Sigma_{t,0} \frac{T_0}{T(x)} \quad (3)$$



Analytical Benchmark

- This analytical benchmark includes
 - S_2 transport: particles restricted to the $\pm x$ direction.
 - Doppler-broadening

$$\sigma_t(x) = \sigma_{t,0} \sqrt{\frac{T_0}{T(x)}} \quad (1)$$

- 1-D thermal expansion

$$\rho(x) = \rho_0 \sqrt{\frac{T_0}{T(x)}} \quad (2)$$

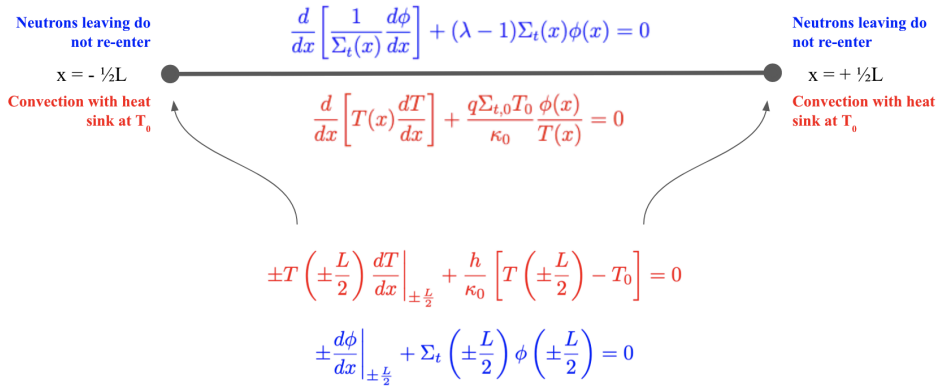
- Using (1) and (2) gives a Doppler-broadened, macroscopic, total cross section that accounts for changes in density due to temperature as

$$\Sigma_t(x) = \frac{\rho_0 \sigma_{t,0} N_A}{A} \frac{T_0}{T(x)} \equiv \Sigma_{t,0} \frac{T_0}{T(x)} \quad (3)$$

- where $\sigma_{t,0}$ is the total microscopic cross section at T_0 , N_A is Avogadro's number, and A is the mass number of the medium.



System Domain, Differential Equations, and Boundary Conditions





System Domain, Differential Equations, and Boundary Conditions

$$\frac{d}{dx} \left[\frac{1}{\Sigma_t(x)} \frac{d\phi}{dx} \right] + (\lambda - 1) \Sigma_t(x) \phi(x) = 0$$

$$\frac{d}{dx} \left[T(x) \frac{dT}{dx} \right] + \frac{q \Sigma_{t,0} T_0}{\kappa_0} \frac{\phi(x)}{T(x)} = 0$$

$$\pm T \left(\pm \frac{L}{2} \right) \frac{dT}{dx} \Big|_{\pm \frac{L}{2}} + \frac{h}{\kappa_0} \left[T \left(\pm \frac{L}{2} \right) - T_0 \right] = 0$$

$$\pm \frac{d\phi}{dx} \Big|_{\pm \frac{L}{2}} + \Sigma_t \left(\pm \frac{L}{2} \right) \phi \left(\pm \frac{L}{2} \right) = 0$$

- The fundamental assumption (ansatz) of [5]: $T(x) = f\phi(x)$. This imposes two constraints that determine h and $\sigma_{t,0}$. The solution is

$$\phi(x) = \phi(0) \sqrt{1 - \frac{(\lambda - 1)P^2 x^2}{L^2 q^2 \phi^2(0)}} \quad \text{WITH} \quad \lambda = \frac{1}{k_{eff}} \frac{\nu \Sigma_f}{\Sigma_t} + \frac{\Sigma_s}{\Sigma_t} \quad (4)$$

- where P is the slab power and L is the slab equilibrium length.

OpenMC Model





OpenMC Model

- Patch to mimic S_2 transport, which restricts particle direction to $\pm x$:



OpenMC Model

- Patch to mimic S_2 transport, which restricts particle direction to $\pm x$:
 - Source direction distribution only $\pm x$. (simulation script)



OpenMC Model

- Patch to mimic S_2 transport, which restricts particle direction to $\pm x$:
 - Source direction distribution only $\pm x$. (simulation script)
 - Scattering samples to either continue forward or backscatter. (source code)



OpenMC Model

- Patch to mimic S_2 transport, which restricts particle direction to $\pm x$:
 - Source direction distribution only $\pm x$. (simulation script)
 - Scattering samples to either continue forward or backscatter. (source code)
 - Particles born from fission also have direction distribution of $\pm x$. (source code)



OpenMC Model

- Patch to mimic S_2 transport, which restricts particle direction to $\pm x$:
 - Source direction distribution only $\pm x$. (simulation script)
 - Scattering samples to either continue forward or backscatter. (source code)
 - Particles born from fission also have direction distribution of $\pm x$. (source code)
- Custom one-group XS temperature library



OpenMC Model

- Patch to mimic S_2 transport, which restricts particle direction to $\pm x$:
 - Source direction distribution only $\pm x$. (simulation script)
 - Scattering samples to either continue forward or backscatter. (source code)
 - Particles born from fission also have direction distribution of $\pm x$. (source code)
- Custom one-group XS temperature library
 - Uses analytical $\Sigma(T)$, instead of explicitly modeling thermal expansion.



OpenMC Model

- Patch to mimic S_2 transport, which restricts particle direction to $\pm x$:
 - Source direction distribution only $\pm x$. (simulation script)
 - Scattering samples to either continue forward or backscatter. (source code)
 - Particles born from fission also have direction distribution of $\pm x$. (source code)
- Custom one-group XS temperature library
 - Uses analytical $\Sigma(T)$, instead of explicitly modeling thermal expansion.
 - Contains data for integer temperatures $T \in [308, 358]$ K.



OpenMC Model

- Patch to mimic S_2 transport, which restricts particle direction to $\pm x$:
 - Source direction distribution only $\pm x$. (simulation script)
 - Scattering samples to either continue forward or backscatter. (source code)
 - Particles born from fission also have direction distribution of $\pm x$. (source code)
- Custom one-group XS temperature library
 - Uses analytical $\Sigma(T)$, instead of explicitly modeling thermal expansion.
 - Contains data for integer temperatures $T \in [308, 358]$ K.
 - Rounds to nearest temperature for lookup between two data points.



OpenMC Model

- Patch to mimic S_2 transport, which restricts particle direction to $\pm x$:
 - Source direction distribution only $\pm x$. (simulation script)
 - Scattering samples to either continue forward or backscatter. (source code)
 - Particles born from fission also have direction distribution of $\pm x$. (source code)
- Custom one-group XS temperature library
 - Uses analytical $\Sigma(T)$, instead of explicitly modeling thermal expansion.
 - Contains data for integer temperatures $T \in [308, 358]$ K.
 - Rounds to nearest temperature for lookup between two data points.
- Mesh deformation is possible in Cardinal via DAGMC [6] but was not available at the time of this work.



OpenMC Model

- Patch to mimic S_2 transport, which restricts particle direction to $\pm x$:
 - Source direction distribution only $\pm x$. (simulation script)
 - Scattering samples to either continue forward or backscatter. (source code)
 - Particles born from fission also have direction distribution of $\pm x$. (source code)
- Custom one-group XS temperature library
 - Uses analytical $\Sigma(T)$, instead of explicitly modeling thermal expansion.
 - Contains data for integer temperatures $T \in [308, 358]$ K.
 - Rounds to nearest temperature for lookup between two data points.
- Mesh deformation is possible in Cardinal via DAGMC [6] but was not available at the time of this work.
- Geometry uses equilibrium length provided from the benchmark $L = 106.47$ cm in the x-direction, 1 cm in the y-direction, and 1 cm in the z-direction.



OpenMC Model

- Patch to mimic S_2 transport, which restricts particle direction to $\pm x$:
 - Source direction distribution only $\pm x$. (simulation script)
 - Scattering samples to either continue forward or backscatter. (source code)
 - Particles born from fission also have direction distribution of $\pm x$. (source code)
- Custom one-group XS temperature library
 - Uses analytical $\Sigma(T)$, instead of explicitly modeling thermal expansion.
 - Contains data for integer temperatures $T \in [308, 358]$ K.
 - Rounds to nearest temperature for lookup between two data points.
- Mesh deformation is possible in Cardinal via DAGMC [6] but was not available at the time of this work.
- Geometry uses equilibrium length provided from the benchmark $L = 106.47$ cm in the x-direction, 1 cm in the y-direction, and 1 cm in the z-direction.
- Divided into N Cartesian cells, $N = [5, 10, 25, 50, 100, 250, 500, 1000]$.

MOOSE Heat Conduction Model





MOOSE Heat Conduction Model

- MOOSE solves for temperature distribution.



MOOSE Heat Conduction Model

- MOOSE solves for temperature distribution.
- Mesh uses identical dimensions as OpenMC model. Allows 1:1 feedback.



MOOSE Heat Conduction Model

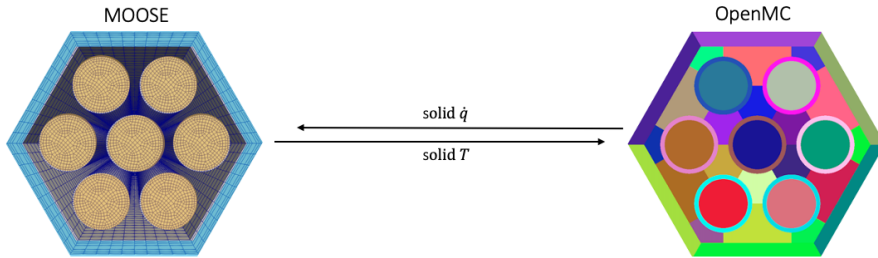
- MOOSE solves for temperature distribution.
- Mesh uses identical dimensions as OpenMC model. Allows 1:1 feedback.
- Jacobi Free Newton Krylov (JFNK) solver.



Coupling, Data Mapping, and Convergence Criteria

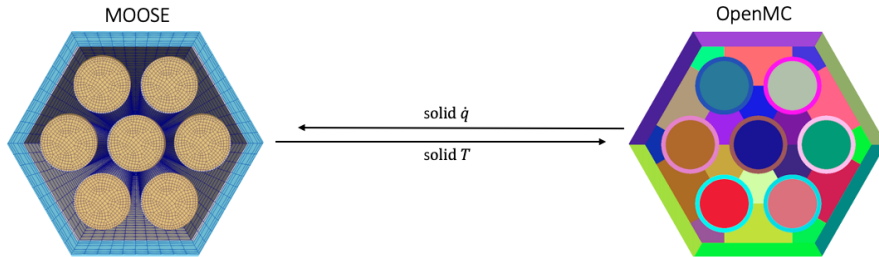


Coupling, Data Mapping, and Convergence Criteria





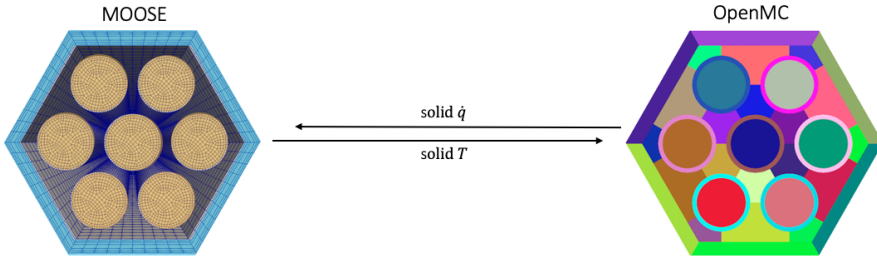
Coupling, Data Mapping, and Convergence Criteria



- 200 Picard Iterations. Robbins-Monro relaxation assisted tally statistics [7].



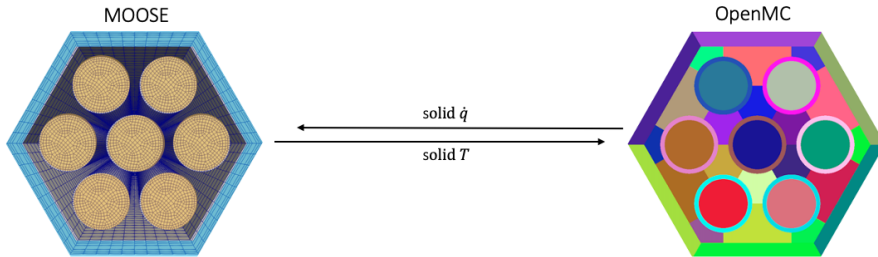
Coupling, Data Mapping, and Convergence Criteria



- 200 Picard Iterations. Robbins-Monro relaxation assisted tally statistics [7].
- k -eigenvalue simulation used 50,000 particles per batch, 50 inactive batches and 100 active batches.



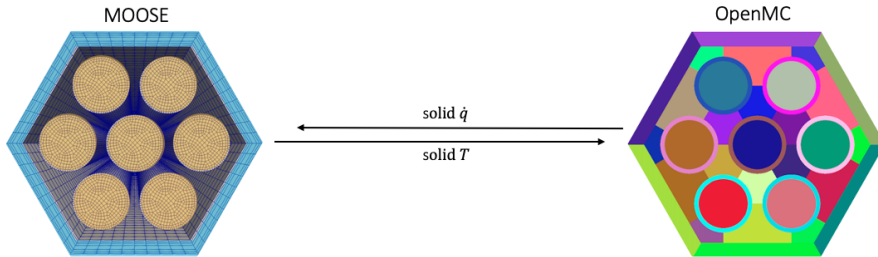
Coupling, Data Mapping, and Convergence Criteria



- 200 Picard Iterations. Robbins-Monro relaxation assisted tally statistics [7].
- k -eigenvalue simulation used 50,000 particles per batch, 50 inactive batches and 100 active batches.
 - Shannon Entropy study confirmed sufficiency following criteria from [8].



Coupling, Data Mapping, and Convergence Criteria



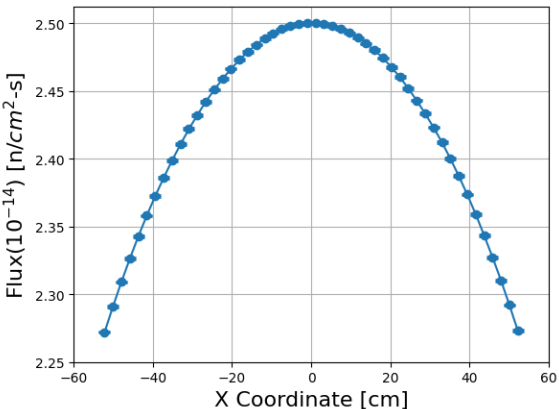
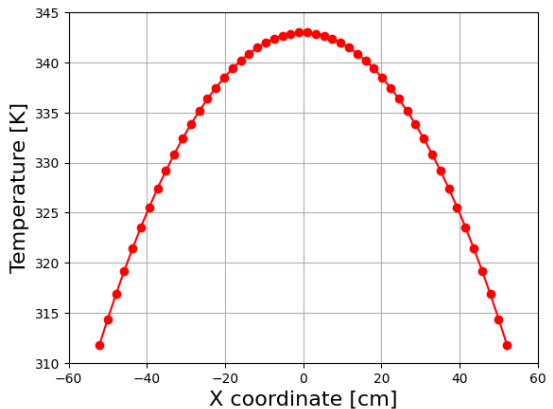
- 200 Picard Iterations. Robbins-Monro relaxation assisted tally statistics [7].
- k -eigenvalue simulation used 50,000 particles per batch, 50 inactive batches and 100 active batches.
 - Shannon Entropy study confirmed sufficiency following criteria from [8].
- Final transport solve with converged temperature used 250,000 particles per batch.



Outputs and Comparisons



Outputs and Comparisons



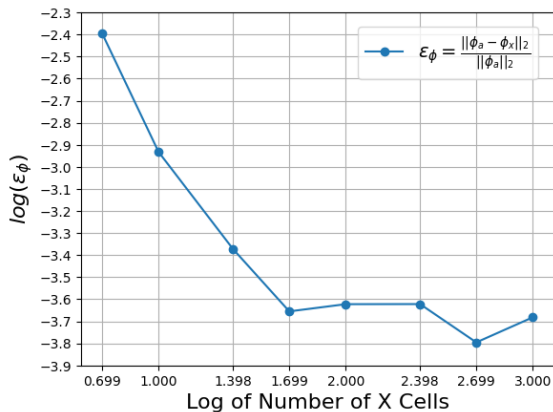
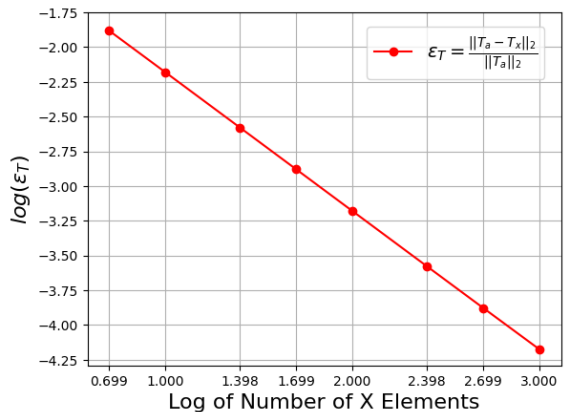
- Numerical solutions for 50 mesh elements. On the right, error bars show the relative error of the flux, which are nearly smaller than the circular marker sizes.



Solution L_2 Error Norms



Solution L_2 Error Norms



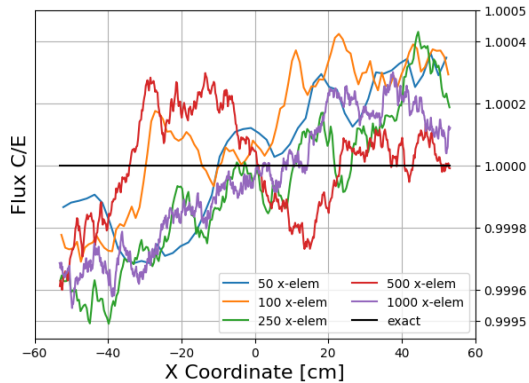
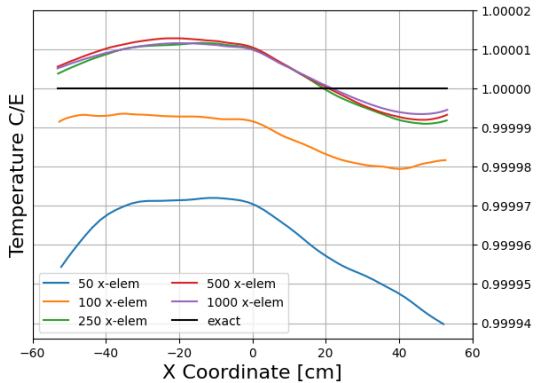
- Error norms as a function of heat conduction mesh element count and OpenMC cell count, respectively. Temperature slope -0.9986 ($R^2 \approx 1.0$).



Computed to Expected Ratios



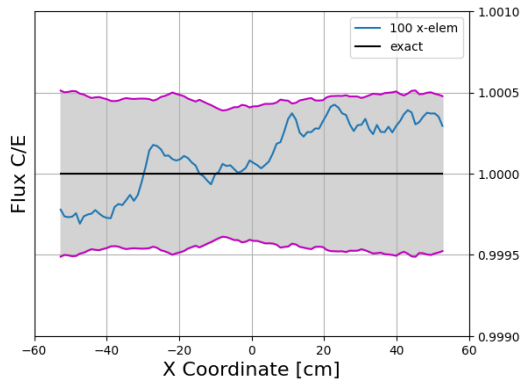
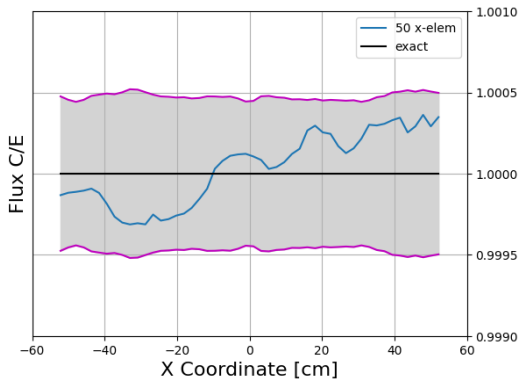
Computed to Expected Ratios



- C/E for fine cases ($N = 50, 100, 250, 500, 1000$). Note the scales of the y-axes - the temperature is everywhere being predicted to within 0.006% and flux is everywhere being predicted to within 0.05%.



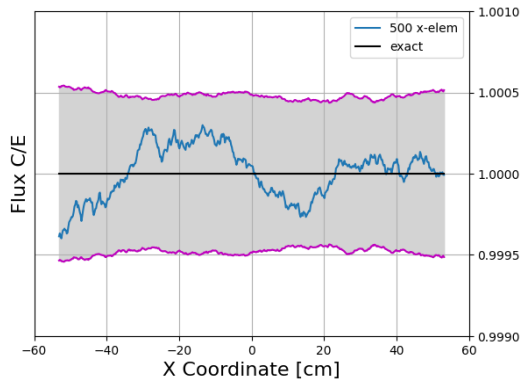
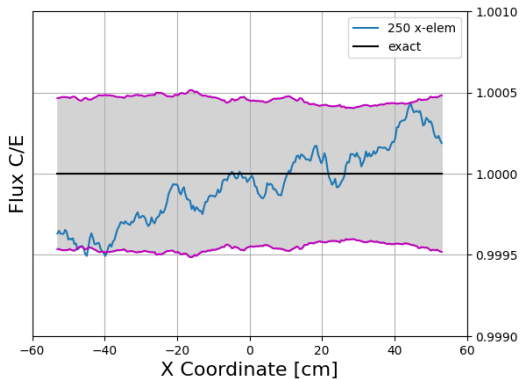
Individual Flux C/E with 2σ Error Bars for Fine Cases



- C/E in blue with 2σ error bars (gray bounded by purple). 50 and 100 cells.



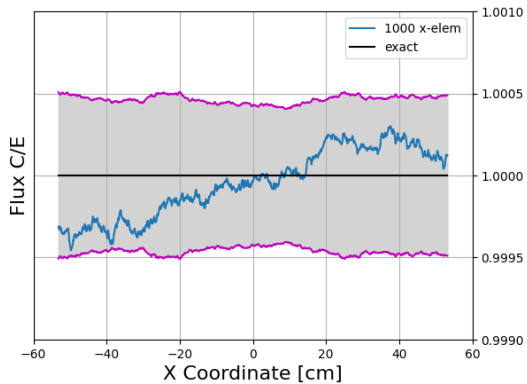
Individual Flux C/E with 2σ Error Bars for Fine Cases



- C/E in blue with 2σ error bars (gray bounded by purple). 250 and 500 cells



Individual Flux C/E with 2σ Error Bars for Fine Cases



- C/E in blue with 2σ error bars (gray bounded by purple). 1000 cells.



Eigenvalue comparisons across each spatial discretization

Resolution	k_{eff}	(numerical - analytical) [pcm]
analytical	0.29557	-
5	0.29624 \pm 0.00003	67 \pm 3
10	0.29581 \pm 0.00004	24 \pm 4
25	0.29563 \pm 0.00004	6 \pm 4
50	0.29553 \pm 0.00004	-4 \pm 4
100	0.29557 \pm 0.00003	0 \pm 3
250	0.29561 \pm 0.00004	4 \pm 4
500	0.29561 \pm 0.00004	4 \pm 4
1000	0.29558 \pm 0.00004	1 \pm 4

- k_{eff} is a system-wide parameter, so it converges much faster than flux and is not as dependent on number of cells.

Summary





Summary

- In this work, we



Summary

- In this work, we
 - compute $T(x)$, $\phi(x)$, and the k -eigenvalue in the slab at its equilibrium length for various mesh counts.



Summary

- In this work, we
 - compute $T(x)$, $\phi(x)$, and the k -eigenvalue in the slab at its equilibrium length for various mesh counts.
 - compare numerical and analytical results via



Summary

- In this work, we
 - compute $T(x)$, $\phi(x)$, and the k -eigenvalue in the slab at its equilibrium length for various mesh counts.
 - compare numerical and analytical results via
 - mesh count vs L_2 error norm plots.



Summary

- In this work, we
 - compute $T(x)$, $\phi(x)$, and the k -eigenvalue in the slab at its equilibrium length for various mesh counts.
 - compare numerical and analytical results via
 - mesh count vs L_2 error norm plots.
 - C/E plots for $T(x)$ and $\phi(x)$.



Summary

- In this work, we
 - compute $T(x)$, $\phi(x)$, and the k -eigenvalue in the slab at its equilibrium length for various mesh counts.
 - compare numerical and analytical results via
 - mesh count vs L_2 error norm plots.
 - C/E plots for $T(x)$ and $\phi(x)$.
 - 2σ error bar plots for each $\phi(x)$ C/E .



Summary

- In this work, we
 - compute $T(x)$, $\phi(x)$, and the k -eigenvalue in the slab at its equilibrium length for various mesh counts.
 - compare numerical and analytical results via
 - mesh count vs L_2 error norm plots.
 - C/E plots for $T(x)$ and $\phi(x)$.
 - 2σ error bar plots for each $\phi(x)$ C/E .
 - eigenvalue pcm difference from analytical.



Summary

- In this work, we
 - compute $T(x)$, $\phi(x)$, and the k -eigenvalue in the slab at its equilibrium length for various mesh counts.
 - compare numerical and analytical results via
 - mesh count vs L_2 error norm plots.
 - C/E plots for $T(x)$ and $\phi(x)$.
 - 2σ error bar plots for each $\phi(x)$ C/E .
 - eigenvalue pcm difference from analytical.
 - verify Cardinal's capability to model this 1-D coupled heat transfer and neutron transport benchmark.



Summary

- In this work, we
 - compute $T(x)$, $\phi(x)$, and the k -eigenvalue in the slab at its equilibrium length for various mesh counts.
 - compare numerical and analytical results via
 - mesh count vs L_2 error norm plots.
 - C/E plots for $T(x)$ and $\phi(x)$.
 - 2σ error bar plots for each $\phi(x)$ C/E .
 - eigenvalue pcm difference from analytical.
 - verify Cardinal's capability to model this 1-D coupled heat transfer and neutron transport benchmark.
- Next steps include



Summary

- In this work, we
 - compute $T(x)$, $\phi(x)$, and the k -eigenvalue in the slab at its equilibrium length for various mesh counts.
 - compare numerical and analytical results via
 - mesh count vs L_2 error norm plots.
 - C/E plots for $T(x)$ and $\phi(x)$.
 - 2σ error bar plots for each $\phi(x)$ C/E .
 - eigenvalue pcm difference from analytical.
 - verify Cardinal's capability to model this 1-D coupled heat transfer and neutron transport benchmark.
- Next steps include
 - simulation using NekRS for heat transfer.



Summary

- In this work, we
 - compute $T(x)$, $\phi(x)$, and the k -eigenvalue in the slab at its equilibrium length for various mesh counts.
 - compare numerical and analytical results via
 - mesh count vs L_2 error norm plots.
 - C/E plots for $T(x)$ and $\phi(x)$.
 - 2σ error bar plots for each $\phi(x)$ C/E .
 - eigenvalue pcm difference from analytical.
 - verify Cardinal's capability to model this 1-D coupled heat transfer and neutron transport benchmark.
- Next steps include
 - simulation using NekRS for heat transfer.
 - explicit modeling of thermal expansion and density feedback.



Summary

- In this work, we
 - compute $T(x)$, $\phi(x)$, and the k -eigenvalue in the slab at its equilibrium length for various mesh counts.
 - compare numerical and analytical results via
 - mesh count vs L_2 error norm plots.
 - C/E plots for $T(x)$ and $\phi(x)$.
 - 2σ error bar plots for each $\phi(x)$ C/E .
 - eigenvalue pcm difference from analytical.
 - verify Cardinal's capability to model this 1-D coupled heat transfer and neutron transport benchmark.
- Next steps include
 - simulation using NekRS for heat transfer.
 - explicit modeling of thermal expansion and density feedback.
 - further investigation into the error norms.



Summary

- In this work, we
 - compute $T(x)$, $\phi(x)$, and the k -eigenvalue in the slab at its equilibrium length for various mesh counts.
 - compare numerical and analytical results via
 - mesh count vs L_2 error norm plots.
 - C/E plots for $T(x)$ and $\phi(x)$.
 - 2σ error bar plots for each $\phi(x)$ C/E .
 - eigenvalue pcm difference from analytical.
 - verify Cardinal's capability to model this 1-D coupled heat transfer and neutron transport benchmark.
- Next steps include
 - simulation using NekRS for heat transfer.
 - explicit modeling of thermal expansion and density feedback.
 - further investigation into the error norms.
 - integration of this benchmark and others [9] into Cardinal's regression testing.

Acknowledgements

- The first author was supported in part by the US Nuclear Regulatory Commission's Graduate Fellowship Program administered by the University of Wisconsin-Madison.
- Co-authors: April J. Novak, Patrick Shriwise, and Paul P.H. Wilson.
- Benchmark authors: David P. Greisheimer and Gabriel Kooreman.
- OpenMC, Cardinal, and MOOSE teams!



Bibliography

- [1] A.J. Novak et al. "Coupled Monte Carlo and Thermal-Fluid Modeling of High Temperature Gas Reactors Using Cardinal". In: *Annals of Nuclear Energy* 177 (2022), p. 109310. DOI: [10.1016/j.anucene.2022.109310](https://doi.org/10.1016/j.anucene.2022.109310).
- [2] P.K. Romano et al. "OpenMC: A State-of-the-Art Monte Carlo Code for Research and Development". In: *Annals of Nuclear Energy* 82 (2015), pp. 90–97. DOI: [10.1016/j.anucene.2014.07.048](https://doi.org/10.1016/j.anucene.2014.07.048).
- [3] P. Fischer et al. *NekRS, a GPU-Accelerated Spectral Element Navier-Stokes Solver*. arXiv:2104.05829. Apr. 2021.
- [4] Alexander D. Lindsay et al. "2.0 - MOOSE: Enabling massively parallel multiphysics simulation". In: *SoftwareX* 20 (2022), p. 101202. ISSN: 2352-7110. DOI: <https://doi.org/10.1016/j.softx.2022.101202>.
- [5] D.P. Griesheimer and G. Kooreman. "Analytical Benchmark Solution for 1-D Neutron Transport Coupled with Thermal Conduction and Material Expansion". In: *Proceedings of M&C*. Pittsburgh, Pennsylvania, 2022.

Bibliography

- [6] A.J. Novak et al. "Multiphysics Coupling of OpenMC CAD-Based Transport to MOOSE using Cardinal and Aurora". In: *Proceedings of M&C*. Niagara Falls, Ontario, Canada, 2023.
- [7] J. Dufek and W. Gudowski. "Stochastic Approximation for Monte Carlo Calculation of Steady-State Conditions in Thermal Reactors". In: *Nuclear Science and Engineering* 152 (2006), pp. 274–283. DOI: [10.13182/NSE06-2](https://doi.org/10.13182/NSE06-2).
- [8] F.B. Brown. "On the Use of Shannon Entropy of the Fission Distribution for Assessing Convergence of Monte Carlo Criticality Calculations". In: *Proceedings of PHYSOR*. Vancouver, British Columbia, Canada, 2006.
- [9] A.H. Hegazy and A.J. Novak. "Verification of the Cardinal Multiphysics Solver with the Doppler Slab Benchmark". In: *Proceedings of M&C*. Niagara Falls, Ontario, Canada, 2023.

Questions?

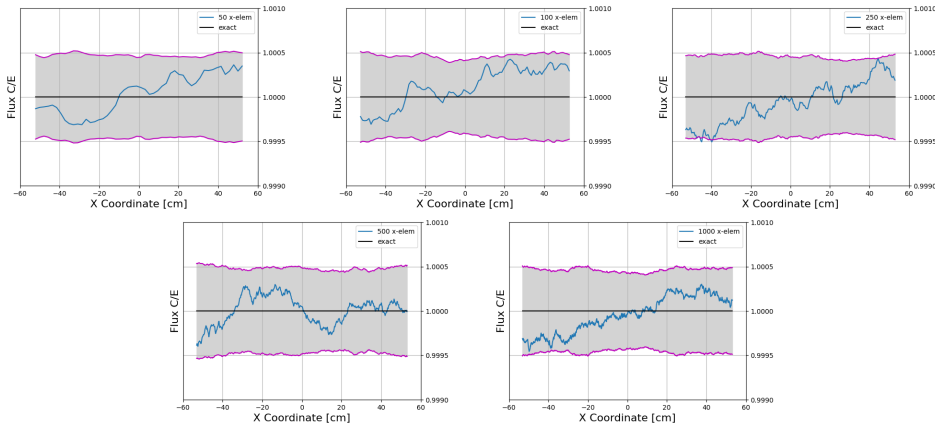
- OpenMC website: <https://openmc.org/>
- OpenMC repository: <https://github.com/openmc-dev/openmc>
- Cardinal website: <https://cardinal.cels.anl.gov>
- Cardinal repository: <https://github.com/neams-th-coe/cardinal.git>
- MOOSE website: <https://mooseframework.inl.gov/>
- MOOSE repository: <https://github.com/idaholab/moose>
- Add me on LinkedIn ([lewisgross1296](#)) and GitHub ([lewisgross1296](#))!



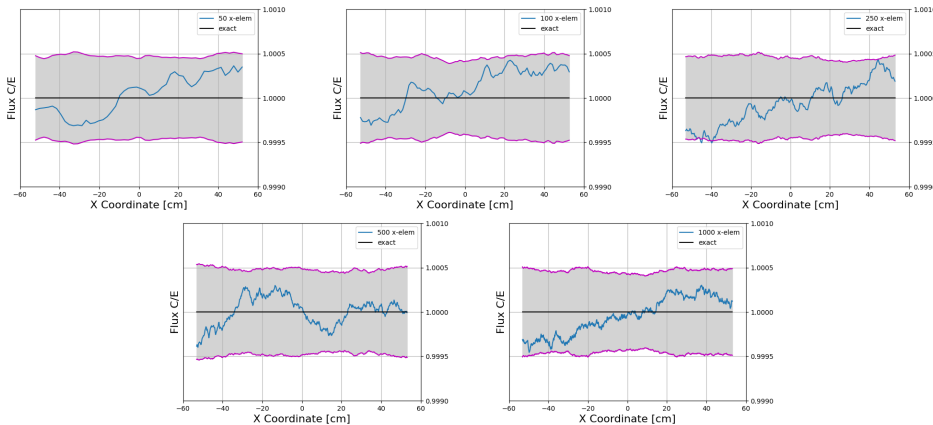
Benchmark Canonical Parameters Values

Parameter	Value	Units
ρ_0	1.2	g/cm ³
L_0	100	cm
A	180	g/mol
T_0	293	K
q	1.0×10^8	eV
P	1.0×10^{22}	eV/s
κ_0	1.25×10^{19}	eV/(s cm K ²)
$\phi(0)$	2.5×10^{14}	1/(s cm ²)
$\nu \Sigma_f / \Sigma_t$	1.5	--
Σ_s / Σ_t	0.45	--

Why do the error bars appear on the same order despite cell refinement?

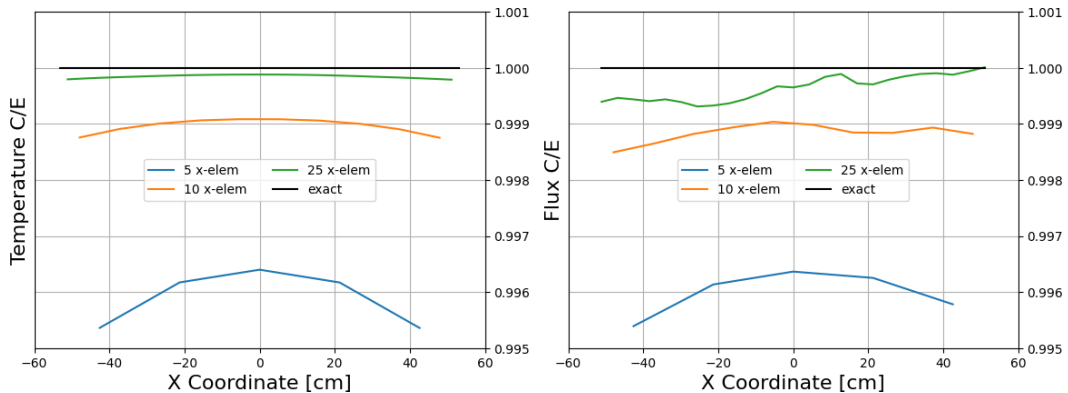


Why do the error bars appear on the same order despite cell refinement?



- MFP $\in [239, 278]$ cm ($L = 106.47$ cm). Spatially uniform birth distribution. Nearly all points fall within 2σ (95% CI), meaning that Cardinal is computing the correct flux within statistical uncertainty.

Coarse C/E results



- C/E for coarse cases ($N = 5, 10, 25$). The coarse cases' errors are a few orders of magnitude larger than the fine cases. A significant improvement in agreement can be seen between each coarse case.

Deriving the Benchmark ODE for $\phi(x)$

- Going from the steady-state, mono-energetic, 1-D neutron transport equation to the ODE that describes neutron transport for this benchmark:

$$\mu \frac{\partial \psi(x, \mu)}{\partial x} + \Sigma_t(x) \psi(x, \mu) = \int_{-1}^1 \frac{1}{2} \left[\Sigma_s(x) + \frac{\nu \Sigma_f(x)}{k_{eff}} \right] \psi(x, \mu') d\mu' \quad (5)$$

For now, lump the fission term into the scattering cross section to get

$$\mu \frac{\partial \psi(x, \mu)}{\partial x} + \Sigma_t(x) \psi(x, \mu) = \int_{-1}^1 \frac{1}{2} \Sigma_s(x) \psi(x, \mu') d\mu' \quad (6)$$

Define the scalar flux and the magnitude of current

$$\phi(x) = \int_{-1}^1 \psi(x, \mu) d\mu \quad \text{AND} \quad J(x) = \int_{-1}^1 \mu \psi(x, \mu) d\mu. \quad (7)$$

Considering S_2 transport means restricting the angular cosine to $\mu = \pm 1$:

$$\psi(x, \mu) = \psi(x, -1) \delta(\mu + 1) + \psi(x, 1) \delta(\mu - 1) \quad (8)$$

Deriving the Benchmark ODE for $\phi(x)$

Now carrying out the integral definitions with S_2 quantities gives

$$\phi(x) = \int_{-1}^1 [\psi(x, -1)\delta(\mu + 1) + \psi(x, 1)\delta(\mu - 1)] d\mu = \psi(x, -1) + \psi(x, 1) \quad (9)$$

and

$$J(x) = \int_{-1}^1 \mu [\psi(x, -1)\delta(\mu + 1) + \psi(x, 1)\delta(\mu - 1)] d\mu = \psi(x, 1) - \psi(x, -1) \quad (10)$$

Evaluating (6) at $\mu = \pm 1$ gives

$$-\frac{\partial \psi(x, -1)}{\partial x} + \Sigma_t(x)\psi(x, -1) = \frac{1}{2}\Sigma_s(x)\phi(x); \quad (11)$$

$$\frac{\partial \psi(x, 1)}{\partial x} + \Sigma_t(x)\psi(x, 1) = \frac{1}{2}\Sigma_s(x)\phi(x). \quad (12)$$

Adding (11) and (12) gives

$$-\frac{\partial \psi(x, -1)}{\partial x} + \frac{\partial \psi(x, 1)}{\partial x} + \Sigma_t(x)(\psi(x, -1) + \psi(x, 1)) = \Sigma_s(x)\phi(x) \quad (13)$$

Deriving the Benchmark ODE for $\phi(x)$

The results for $\phi(x)$ and $J(x)$ can simplify (13)

$$\frac{dJ(x)}{dx} + \Sigma_t(x)\phi(x) = \Sigma_s(x)\phi(x) \quad (14)$$

Subtracting (11) and (12) gives

$$-\frac{\partial\psi(x, -1)}{\partial x} - \frac{\partial\psi(x, 1)}{\partial x} + \Sigma_t(x)(\psi(x, -1) - \Sigma_t(x)\psi(x, 1)) = 0 \quad (15)$$

Which can be transformed with similar tricks to

$$\frac{d\phi(x)}{dx} + \Sigma_t(x)J(x) = 0 \quad \text{OR} \quad J(x) = -\frac{1}{\Sigma_t(x)} \frac{d\phi(x)}{dx} \quad (16)$$

Since $\frac{dJ(x)}{dx}$ appears in (14), we can take the derivative of both sides of (16) and substitute it in

$$\frac{dJ(x)}{dx} = -\frac{d}{dx} \left[\frac{1}{\Sigma_t(x)} \frac{d\phi(x)}{dx} \right] \quad (17)$$

Deriving the Benchmark ODE for $\phi(x)$

Now the equation that only depends on $\phi(x)$ is given by

$$-\frac{d}{dx} \left[\frac{1}{\Sigma_t(x)} \frac{d\phi(x)}{dx} \right] + \Sigma_t(x)\phi(x) = \Sigma_s(x)\phi(x) \quad (18)$$

At this point, we “un-lump” the scattering cross section to write out the fission term

$$-\frac{d}{dx} \left[\frac{1}{\Sigma_t(x)} \frac{d\phi(x)}{dx} \right] + \Sigma_t(x)\phi(x) - \left[\Sigma_s(x) + \frac{\nu\Sigma_f}{k_{eff}} \right] \phi(x) = 0 \quad (19)$$

$$\frac{d}{dx} \left[\frac{1}{\Sigma_t(x)} \frac{d\phi(x)}{dx} \right] + \Sigma_t(x) \left[\frac{\Sigma_s(x) + \frac{\nu\Sigma_f}{k_{eff}}}{\Sigma_t} - 1 \right] \phi(x) = 0 \quad (20)$$

Now define

$$\lambda \equiv \frac{\Sigma_s(x) + \frac{\nu\Sigma_f}{k_{eff}}}{\Sigma_t} \quad (21)$$

giving the final result:

$$\frac{d}{dx} \left[\frac{1}{\Sigma_t(x)} \frac{d\phi(x)}{dx} \right] + \Sigma_t(x)(\lambda - 1)\phi(x) = 0 \quad (22)$$

Deriving the Benchmark ODE for $\phi(x)$

The next task is to apply boundary conditions so that $\phi(x)$ can be specified. In discrete ordinates with $\mu = \pm 1$ (S_2), we use the vacuum boundary condition. The angular flux for positive angular cosines is zero at the left boundary and is zero for negative angular cosines at the right boundary. Using the previous results for $\phi(x)$ and $J(x)$ at the boundaries gives

$$\begin{aligned}\phi(x = \frac{L}{2}) &= \psi(x = \frac{L}{2}, \mu = -1) + \psi(x = \frac{L}{2}, \mu = 1) \quad \text{AND} \\ \phi(x = -\frac{L}{2}) &= \psi(x = -\frac{L}{2}, \mu = -1) + \psi(x = -\frac{L}{2}, \mu = 1)\end{aligned}\quad (23)$$

and

$$\begin{aligned}J(x = \frac{L}{2}) &= -\psi(x = \frac{L}{2}, -1) + \psi(x = \frac{L}{2}, 1) \quad \text{AND} \\ J(x = -\frac{L}{2}) &= -\psi(x = -\frac{L}{2}, -1) + \psi(x = -\frac{L}{2}, 1)\end{aligned}\quad (24)$$

Deriving the Benchmark ODE for $\phi(x)$

Now, terms can be crossed out due to vacuum boundaries. This gives that

$$\phi(x = \frac{L}{2}) = \psi(x = \frac{L}{2}, \mu = 1) \quad \text{AND}$$

$$\phi(x = -\frac{L}{2}) = \psi(x = -\frac{L}{2}, \mu = -1) \quad (25)$$

$$J(x = \frac{L}{2}) = \psi(x = \frac{L}{2}, \mu = 1) \quad \text{AND}$$

$$J(x = -\frac{L}{2}) = -\psi(x = -\frac{L}{2}, \mu = -1) \quad (26)$$

Using this with (16) gives the desired boundary conditions

$$J(x = \pm \frac{L}{2}) = \pm \phi(x = \pm \frac{L}{2}) \quad (27)$$

And the boundary conditions of interest are now

$$\pm \left. \frac{d\phi}{dx} \right|_{x=\pm \frac{L}{2}} + \Sigma_t(x = \pm \frac{L}{2}) \phi(x = \pm \frac{L}{2}) = 0 \quad (28)$$



Analytical Benchmark ODEs

- Based on 1-D S_2 transport, the neutron flux $\phi(x)$ is governed by

$$\frac{d}{dx} \left[\frac{1}{\Sigma_t(x)} \frac{d\phi(x)}{dx} \right] + \Sigma_t(x) (\lambda - 1) \phi(x) = 0 \quad \text{WITH} \\ \pm \frac{d\phi}{dx} \Big|_{x=\pm\frac{L}{2}} + \Sigma_t(x = \pm\frac{L}{2}) \phi(x = \pm\frac{L}{2}) = 0 \quad (29)$$

- $\lambda \equiv \left(\frac{1}{k_{\text{eff}}} \frac{\nu \Sigma_f}{\Sigma_t} + \frac{\Sigma_s}{\Sigma_t} \right)$ [5].
- The conduction equation governs energy conservation in the slab

$$\frac{d}{dx} \left[\kappa(T) \frac{dT(x)}{dx} \right] + q \Sigma_t(x) \phi(x) = 0 \quad \text{WITH} \\ - \kappa(T) \frac{dT}{dx} \Big|_{\pm\frac{L}{2}} = \pm h \left[T(\pm\frac{L}{2}) - T_0 \right] \quad (30)$$

- where κ is the thermal conductivity, q is the energy released **per reaction**, Σ_t is the total macroscopic cross section, and h is the heat transfer coefficient.

Ensuring Validity of the Fundamental Ansatz $T = f\phi(x)$

- Taking the heat conduction ODE

$$\frac{d}{dx} \left[\kappa(T(x)) \frac{dT(x)}{dx} \right] + q \Sigma_t(x) \phi(x) = 0 \quad (31)$$

and using the thermal conductivity and cross section temperature dependence

$$\frac{d}{dx} \left[\kappa_0 T(x) \frac{dT(x)}{dx} \right] + q \Sigma_{t,0} \frac{T_0}{T(x)} \phi(x) = 0 \quad (32)$$

- Taking the neutron transport ODE

$$\frac{d}{dx} \left[\frac{1}{\Sigma_t(x)} \frac{d\phi(x)}{dx} \right] + \Sigma_t(x) (\lambda - 1) \phi(x) = 0 \quad (33)$$

and inserting cross section temperature dependence gives

$$\frac{d}{dx} \left[\frac{T(x)}{\Sigma_{t,0} T_0} \frac{d\phi(x)}{dx} \right] + \Sigma_{t,0} \frac{T_0}{T(x)} (\lambda - 1) \phi(x) = 0 \quad (34)$$

Ensuring Validity of the Fundamental Ansatz $T = f\phi(x)$

- These two equations are very close, and after some re-arranging, they look even closer

$$\frac{d}{dx} \left[T(x) \frac{dT(x)}{dx} \right] + \frac{q\Sigma_{t,0}}{\kappa_0} \frac{T_0}{T(x)} \phi(x) = 0 \quad \text{AND}$$

$$\frac{d}{dx} \left[\frac{T(x)}{\Sigma_{t,0} T_0} \frac{d\phi(x)}{dx} \right] + \Sigma_{t,0} \frac{T_0}{T(x)} (\lambda - 1) \phi(x) = 0 \quad (35)$$

- Applying the ansatz $T(x) = f\phi(x)$ gives

$$\frac{d}{dx} \left[f^2 \phi(x) \frac{d\phi(x)}{dx} \right] + \frac{q\Sigma_{t,0}}{\kappa_0} \frac{T_0}{f} = 0 \quad \text{AND}$$

$$\frac{d}{dx} \left[\frac{f\phi(x)}{\Sigma_{t,0} T_0} \frac{d\phi(x)}{dx} \right] + \Sigma_{t,0} \frac{T_0}{f} (\lambda - 1) = 0 \quad (36)$$

$$\frac{d}{dx} \left[\phi(x) \frac{d\phi(x)}{dx} \right] + \frac{q\Sigma_{t,0}}{\kappa_0} \frac{T_0}{f^3} = 0 \quad \text{AND}$$

$$\frac{d}{dx} \left[\phi(x) \frac{d\phi(x)}{dx} \right] + \left(\Sigma_{t,0} \frac{T_0}{f} \right)^2 (\lambda - 1) = 0 \quad (37)$$

Ensuring Validity of the Fundamental Ansatz $T = f\phi(x)$

- In order to make the ansatz hold, this implies that

$$\frac{q\Sigma_{t,0}}{\kappa_0} \frac{T_0}{f^3} = \left(\Sigma_{t,0} \frac{T_0}{f} \right)^2 (\lambda - 1) \quad \text{OR} \quad \Sigma_{t,0} = \frac{q}{(\lambda - 1)\kappa_0 T_0 f} \quad (38)$$

which is a condition for the total cross section based on system parameters.

- A similar process of matching coefficients must be applied to the boundary conditions to gain a condition for the heat transfer coefficient. Though, at this point, realize that

$$\frac{d}{dx} \left[\phi(x) \frac{d\phi(x)}{dx} \right] + \left(\Sigma_{t,0} \frac{T_0}{f} \right)^2 (\lambda - 1) = 0 \quad (39)$$

- is a separable ODE that can be solved for an analytical solution. The result for the heat transfer coefficient is given by

$$h \left(\sqrt{\frac{L(\lambda - 1)}{\kappa_0 P}} - \frac{2T_0}{P} \right) = 1 \quad (40)$$